ELSEVIER

Thin Solid Films 407 (2002) 215–220

thin solid films

www.elsevier.com/locate/tsf

Effect of electrostatic waves on a rf field penetration into highly collisional helicon plasmas

Shunjiro Shinohara[a,*], Konstantin P. Shamrai[b]

[a]*Interdisciplinary Graduate School of Engineering Sciences, Kyushu University, Kasuga, Fukuoka 816-8580, Japan*
[b]*Scientific Center Institute for Nuclear Research, National Academy of Sciences, Kiev 03680, Ukraine*

Abstract

The spatial distribution is examined of the azimuthal plasma current in highly collisional helicon plasma excited by $m=0$ antenna. The sheath of intense plasma current is shown to arise underneath the antenna due to the generation of strongly damped electrostatic Trivelpiece–Gould waves via mode conversion of the helicon waves. The radial width of the sheath is substantially smaller than the collisional skin size and drops inversely proportionally to the external magnetic field. The dependence of the plasma load resistance on density saturates when the plasma countercurrent becomes strong enough to cancel the antenna fields in the plasma interior. Computed resistance is shown to agree well with measured values under various conditions.

Keywords: Helicon plasma; Rf field; Skin effect; Plasma resistance

1. Introduction

The helicon plasma source is a type of magnetic field enhanced ICP (inductively coupled plasma) which can produce plasmas of the highest densities as compared with other high-density plasma sources [1,2]. It was shown to serve as an efficient plasma tool for various materials processing technologies, including the fabrication of high-quality thin films for electronic, optical and other applications. Helicon plasmas were successfully used for the deposition of amorphous carbon [3], silica (SiO_2) [4–6], cubic boron nitride [7,8], carbon nitride [9], and SiOF [10] films, as well as titania/silica (TiO_2/SiO_2) multilayer films [11], etc.

The efficiency of plasma production in an inductive source substantially depends on that how the electromagnetic fields generated by the external rf driver (antenna) penetrate into the plasma. In a conventional ICP that operates without an external magnetic field, the a.c. fields penetrate into plasma as damped electromagnetic oscillations with the depth determined by the collisional or anomalous skin size. A skin effect is known to arise due to the countercurrent induced in plasma, which cancels the external magnetic flux from the antenna. The plasma load resistance for the ICP can be estimated with a simple transformer model in which the antenna and the sheath of the plasma countercurrent are considered, respectively, as the primary and secondary windings [12]. With the external d.c. magnetic field imposed, the plasma becomes transparent for various waves, which substantially affect the penetration of the rf fields. At low collisionality, $\nu_e \ll \omega$ where ν_e is the electron collision frequency and ω is the driving frequency, the waves penetrate deeply into the plasma and can form the complex countercurrent patterns. At high collisionality, $\nu_e \gtrsim \omega$, the waves are normally strongly damped, and thus can result in a modified skin effect.

In dense helicon plasmas, waves of two kinds can propagate. Electromagnetic helicon waves are weakly damped and deeply penetrate into the plasma even at high collisionality. On the contrary, quasi-electrostatic Trivelpiece–Gould (TG) waves, which arise due to the mode conversion of helicon waves, are strongly damped [13,14]. In the present paper, we examine the effect of the TG wave generation on the penetration of electromagnetic fields into dense helicon plasmas at high collisionality.

*Corresponding author. Tel.: +81-92-5837649; fax: +81-92-5718894.

E-mail address: sinohara@aees.kyushu-u.ac.jp (S. Shinohara), kshamrai@kinr.kiev.ua (K.P. Shamrai).

0040-6090/02/$ - see front matter
PII: S0040-6090(02)00041-X

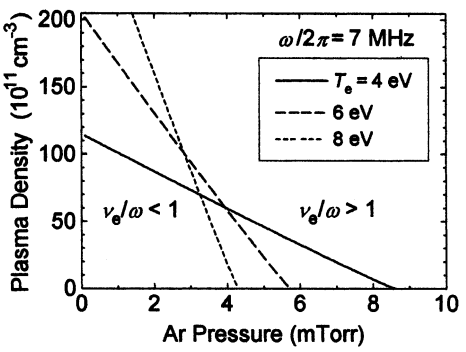

Fig. 1. Curves $\nu_e = \omega$ at various electron temperatures. Ar plasma and $\omega/2\pi = 7$ MHz.

2. Theoretical model and wave spectra

We consider a 5-cm diameter, long plasma source excited by an $m=0$ antenna at a frequency of 7 MHz [15]. The antenna consists of two loops of radius $r_A =$ 3 cm, of axial width and separation equal to 1 cm, and with parallel or anti-parallel currents. The source operates at high Ar pressures either in the ICP mode, $\omega_{ce} < \nu_e$, or in the helicon mode, $\omega_{ce} > \nu_e$ where ω_{ce} is the electron cyclotron frequency and the electron collision frequency, ν_e, accounts for both electron–neutral and electron–ion collisions. The regions of low and high collisionality are shown in Fig. 1 on the plasma density–Ar pressure plane. A theoretical model for the calculation of the fields excitation and rf power absorption in the source was described and shown to give a satisfactory agreement with measurements in our recent paper [16]. In computations, the source is considered as a plasma column of length $L=160$ cm ($z=0$ is the column midplane) and radius $r_0=2.5$ cm; the antenna of real geometry is positioned at $z_A=-20$ cm. For the present consideration, the radial plasma non-uniformity was taken into account in the form:

$$n(r) = n_0 - (n_0 - n_{edge})(r/r_0)^2 \quad (1)$$

where n_0 is the center density, and the edge density, n_{edge}, can vary from 0 to n_0. The model density profile, as given by Eq. (1), seems to be relevant for these experimental conditions. This is confirmed by the profiles measured 2 cm from the antenna midplane (see Fig. 5 in Shinohara and Shamrai [16]), that is within or at least quite close to the region where the most intense currents are excited, and thus, a principal power deposition occurs. Computations were performed for specific conditions of experiments [17], at a high Ar pressure of 51 mtorr. Hereafter, the currents in the antenna loops are supposed to have parallel directions if the contrary is not mentioned.

An example of the wave spectra for highly collisional ($\nu_e/\omega \approx 6$), unbounded plasma is shown in Fig. 2. Computations were performed using the biquadratic dispersion relation in the uniform, cold-plasma approximation [18]. One can see in Fig. 2 the branch of weakly damped helicon waves (H) and that of strongly damped TG waves. Their penetration depths across the magnetic field, $1/\mathrm{Im}k_\perp$, are, respectively, lower and higher than the collisional skin depth, $\delta_c \approx (c/\omega_{pe})(2\nu_e/\omega)^{1/2}$ where ω_{pe} is the plasma frequency and c is the speed of light. At $k_{||}=0$, both waves merge into mode which describes the penetration, by the depth δ_c, of an axially uniform electromagnetic field [19]. Note that strong collisions substantially modify the dispersion (see Shamrai and Shinohara [19] for more details). In particular, the left ends of dispersion curves in Fig. 2 are near $1/\delta_c$, and thus go down with increasing collision frequency.

Helicon waves in discharge plasmas are excited directly by the driving antenna and deposit the power through both collisional damping and the mode conversion into strongly damped Trivelpiece–Gould (TG) waves [13]. The collisional absorption of helicons is distributed over a broad area of the bulk plasma, whereas the excitation of the TG waves provides a principal part of absorption, which is located near the plasma edge and in the regions of strong density gradient. At high collisions, the power absorption profiles strongly peak in the edge region underneath the antenna [19]. We discuss below the spatial distributions of plasma currents and shielding effect of these currents on penetrating rf fields.

3. Plasma currents

Consider first the currents induced by the antenna in uniform plasma. For the ICP mode ($B_0=0$), the distribution of the azimuthal current density is shown in Fig. 3 by contours spaced by 1/10 of the maximum value of the azimuthal current density, $|j_\theta|_{max}$. The radial width of the current sheath is approximately equal to the skin size, δ_c, and slowly decreases with density. The axial width is practically independent of the density, as it is determined mainly by the total antenna length and its radius.

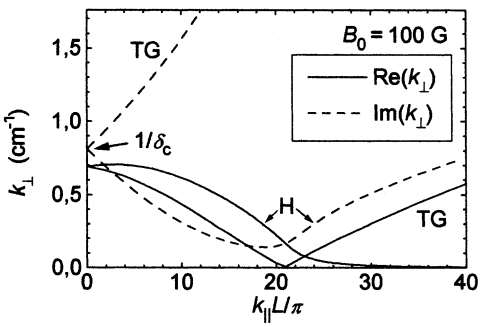

Fig. 2. Computed dispersion curves for the helicon (H) and Trivelpiece–Gould (TG) waves at $p_{Ar}=51$ mtorr, $B_0=100$ G, and $n_0 = 2\times10^{12}$ cm^{-3}.

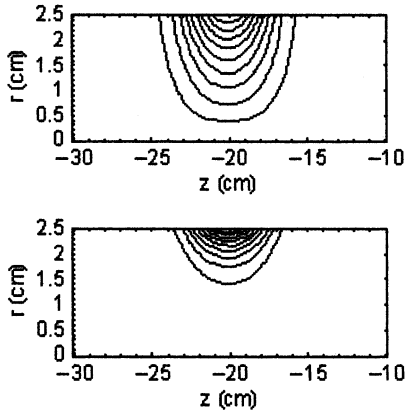

Fig. 3. Contour plots of the azimuthal current density in uniform ICP plasma ($B_0=0$ G), at $p_{Ar}=51$ mtorr and $n_0=2\times10^{12}$ cm^{-3} (top) and 2×10^{13} cm^{-3} (bottom).

In the helicon mode, the plasma current is mainly associated with the $E\times B_0$ drift of electrons in the wave field, $j_\theta \approx -(en_0c/B_0)E_r$ where E_r is the radial component of the ac electric field. Near the plasma boundary, the radial field of the short TG waves is much stronger than the helicon field, $E_r^{(TG)} \approx (\omega_{ce}/\nu_e)E_\theta^{(H)}$ [13]. Therefore, a narrow near-edge sheath of the intense current, which is seen in Fig. 4, is generated by strongly damped TG waves. Note that peaked distribution of $|j_\theta|$ is similar to the distribution of the absorbed power [19]. The radial width of the current sheath is substantially smaller than the collisional skin size as it is determined by the TG damping length averaged over the spectrum. The axial width is approximately equal to that for the ICP mode. In addition to the edge TG current sheath, one can see in Fig. 4 a weak 'halo' resulting from irradiated helicon waves. It was found to extend from the antenna with increasing magnetic field, whereas it shrank with increasing density because the inverse damping length of the helicon wave scales as $\mathrm{Im}k_\perp \propto \nu_e n_0^2/B_0^3 k_\parallel^3$ [13]. The radial size of halo can be estimated from this formula with $k_{||}$ replaced by a mean spectral value of axial wavenumber, $\propto (n_0/B_0)^{1/2}$ [19], so that it scales as $B_0^{3/2}/\nu_e n_0^{1/2}$.

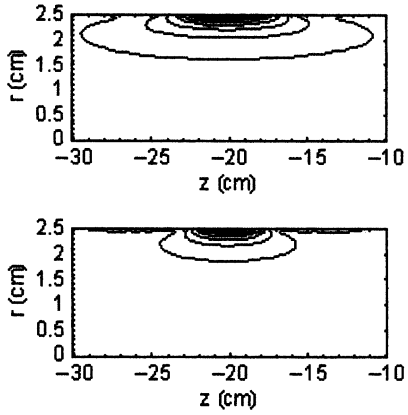

Fig. 4. Contour plots of the azimuthal current density in uniform helicon plasma, at $B_0=300$ G. Other conditions are the same as in Fig. 3.

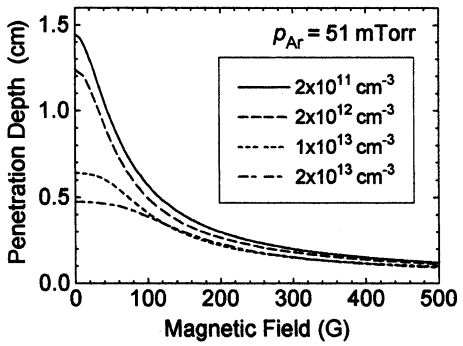

Fig. 5. Radial depth of the current sheath in uniform plasma vs. magnetic field, at various densities.

The radial width of the current sheath, δ_r, was computed as the length of e-fold current drop along the radius in the antenna midplane. It is plotted in Fig. 5 as a function of magnetic field, for various plasma densities. At zero magnetic field (ICP mode), the penetration depth depends very slightly on density below 2×10^{12} cm^{-3} because the collisional skin depth, δ_c, is larger than or of the order of plasma radius. At higher densities, the penetration depth becomes less than r_0 and drops with increasing density more slowly than $n_0^{-1/2}$ as long as it scales as $\delta_c \propto (\nu_e/n_0)^{1/2}$ where ν_e increases with density through the Coulomb collisions. As seen from Fig. 5, the penetration depth is practically independent of density at $B_0>100$ G and decreases with increasing magnetic field, to approximately $1/B_0$. This dependence is clear from Fig. 6 where δ_r, normalized by the electron Larmour radius, ρ_e, is plotted as a function of the plasma density, for various magnetic fields. As seen, $\delta_r \approx 10\rho_e$ over a broad range of the magnetic fields and plasma densities. Note that $\rho_e \approx 0.5$ mm at $B_0=100$ G and $T_e=4$ eV. The axial width of the current sheath, δ_z,

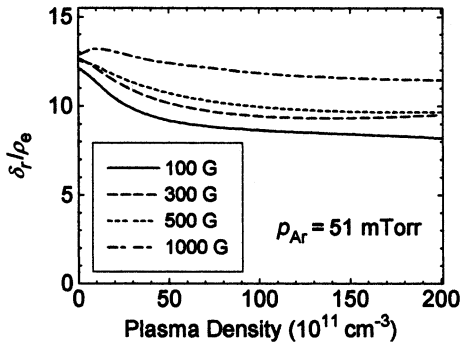

Fig. 6. Radial depth of the current sheath normalized by the electron Larmour radius, for the uniform plasma and various magnetic fields.

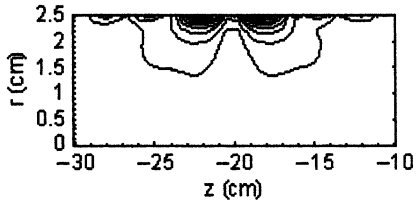

Fig. 7. Contour plots of the azimuthal current density in uniform plasma excited with anti-parallel antenna currents, at $B_0=100$ G and $n_0=1\times10^{13}$ cm^{-3}.

depends mainly on the antenna geometry and was computed to make 4–6 cm at any parameters.

The radial width of the current sheath can be estimated as the inverse imaginary part of the perpendicular TG wavenumber, $\mathrm{Im}k_{\perp}^{(\mathrm{TG})}\approx k_{\|}\nu_e\omega_{ce}(\omega^2+\nu_e^2)^{-1}$ [13], with $k_{||}$ substituted by some characteristic value, k. Inasmuch as the current sheath arises as a plasma response to the antenna field, k is of order of the inverse characteristic length for the vacuum antenna field drop in z-direction. If a single-loop antenna is axially thin, $\bar{k}\sim r_A^{-1}$. In our case of axially extended double-loop antenna, k is found to be somewhat less, $\sim\delta_z^{-1}<r_A^{-1}$. Finally, at high collisions under consideration, $\nu_e\gg\omega$, one arrives at the following estimation, $\delta_r/\rho_e\approx\delta_z\nu_e/v_{Te}=\delta_z/l_e$ where v_{Te} and l_e are the electron thermal velocity and mean free path, respectively. This estimation is found to be in a good agreement with computed data presented in Fig. 6.

The distribution of the current density for the anti-parallel currents in the antenna loops is shown in Fig. 7. It consists of two rings with opposite currents and is strongly localized under the antenna at various parameters. The 'halo' is suppressed in this case as a result of reduced radiation of the helicon waves.

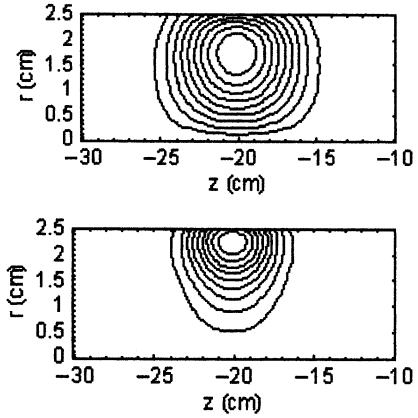

Fig. 8. The same as in Fig. 3 but for the nonuniform plasma with $n_{edge}=0.2n_0$.

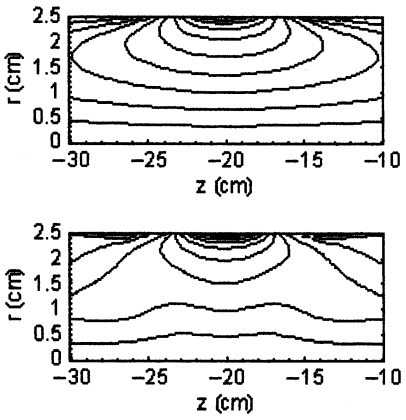

Fig. 9. The same as in Fig. 4 but for the nonuniform plasma with $n_{edge}=0.2n_0$.

4. Effect of the plasma non-uniformity

The plasma non-uniformity results in decrease of the current density magnitude and in extension of the current sheath from the plasma boundary as well as in substantial extension from the antenna of the helicon 'halo'. At some critical ratio of n_{edge}/n_0, which decreases with increase of the central density and magnetic field, the current peak shifts from the edge into the bulk plasma. For the ICP mode, this effect is shown in Fig. 8 computed for the non-uniform plasma with radial profile given by Eq. (1), and for the same central density as seen in Fig. 3, but for $n_{edge}=0.2n_0$. In the helicon mode, the amplitudes of the TG waves arising due to the edge mode conversion are so high as to keep the current peak at the plasma boundary, even at low edge density, as seen in Fig. 9. The helicon current 'halo' in non-uniform plasma extends from the antenna due to enhanced helicon radiation, as far as damping of helicons decreases with density. At very low edge densities, the edge mode conversion strongly decreases whereas the bulk mode conversion increases, and the current peak is found inside the plasma.

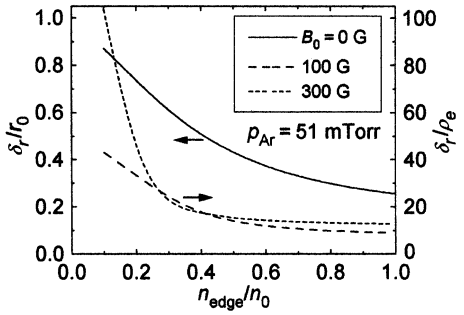

Fig. 10. Dependences of the radial penetration depth on edge-to-center density ratio, at fixed center density $n_0=1\times10^{13}$ cm^{-3} and various magnetic fields.

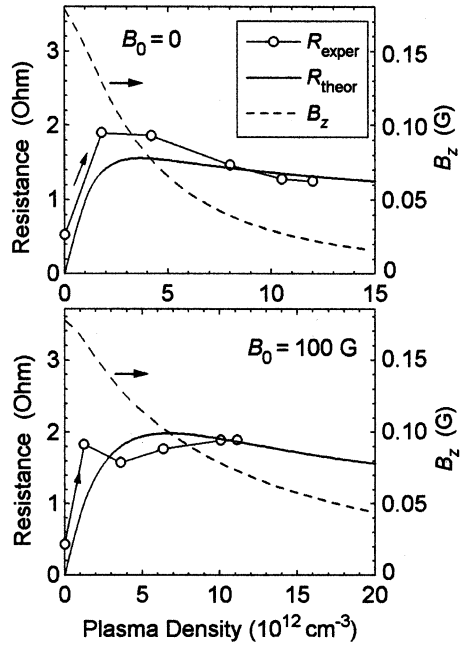

Fig. 11. Computed plasma resistance and measured antenna load resistance, and the absolute value of the magnetic field on the axis in the antenna midplane, for the ICP (top) and helicon plasma at 100 G (bottom), at $n_{edge}=0.5n_0$.

The variation of the radial width of current sheath, δ_r, with the edge density is shown in Fig. 10, for both ICP and helicon modes. One can see that the penetration depth increases with decreasing edge density, and the rate of increase grows with magnetic field at low edge densities. In the ICP mode, the increase of the penetration depth originates in the decrease of plasma density, and thus, in the decrease of shielding effect of the plasma current, as the latter is proportional to the density. In helicon mode, there is another primary reason for the rapid increase of the penetration depth with decreasing edge density: the generation of TG waves via bulk mode conversion. With the increase in density gradient, the intensity of the bulk mode conversion increases and the region of the TG wave generation spreads from the plasma edge into the bulk plasma.

5. Plasma load resistance

The load impedance of the driving antenna is the sum of the impedance introduced by the radiation of damping waves into plasma (plasma impedance) and that determined by losses in the rf circuit and metal environment. Computed plasma resistance for the ICP mode is shown as a function of the central plasma density at the top of Fig. 11. One can see that the resistance increases, saturates at some characteristic value of density, and then slowly drops. The saturation occurs when the plasma countercurrent becomes strong enough to substantially reduce the fields in the plasma interior. Fig. 11 also shows plots of the amplitude of the axial magnetic field on the axis in the antenna midplane, $|B_z(r=0,\ z=z_A)|$, computed with 1 A current in each of the antenna loops. As can be seen, at the saturation point, the magnetic field drops approximately twice as compared with the vacuum (without plasma) value. At this point $\delta_c \approx r_0/2$. Measured antenna load resistance (open circles) agrees well with computation. The density jump shown by the arrow at the experimental curve occurs from the low-density mode to the high density in the vicinity of the resistance maximum.

The plasma resistance computed for the helicon mode at 100 G is shown at the bottom of Fig. 11. Its magnitude is of the same order as it is in the ICP case, but the saturation occurs at a higher characteristic density. This can be understood by considering a substantial reduction of the area of plasma countercurrent sheath, as is clear from Fig. 4. As seen from the bottom of Fig. 11, the magnetic field on axis also reduces with density, but more slowly as compared with the ICP case. The measured resistance fits well to the computed curve. The measured density jump occurs at a lower density than that at which the resistance reaches a maximum value.

Fig. 12 shows the measured and computed resistances for the high magnetic field of 500 G (top) and for the case of anti-parallel antenna currents (bottom). As seen, the agreement of theory with measurements is pretty

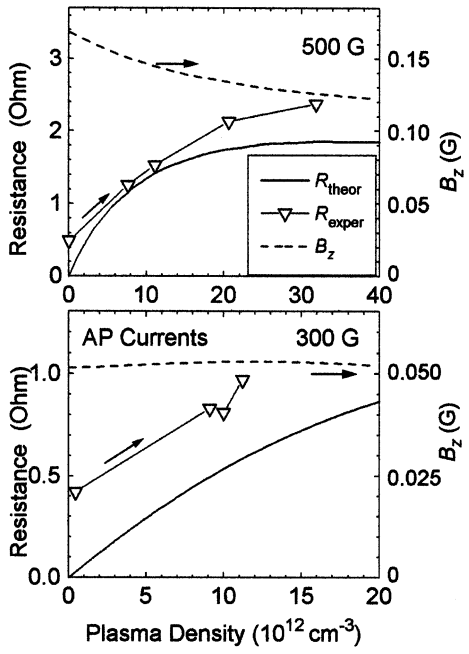

Fig. 12. The same as in Fig. 11, but for $B_0=500$ G and $n_{edge}=0.2n_0$ (top) and $B_0=300$ G and $n_{edge}=n_0$ with anti-parallel excitation (bottom).

good in both cases. The resistance curves saturate at extremely high values of density, as long as the areas of plasma countercurrent sheaths are very small in both cases. Under these conditions, the jumps occur at densities which are much smaller than the maximum value, and the fields on the axis change only slightly over the entire region of density in Fig. 12.

6. Conclusions

The TG waves generated via the mode conversion of helicon waves in highly collisional helicon plasma are shown to induce a strong plasma current localized near the plasma edge underneath the antenna (countercurrent). The radial size of the current area is smaller than the collisional skin size, in a degree inversely proportional to the magnetic field, and depends very slightly on the plasma density. The axial size of the current area depends on the antenna geometry only. The currents associated with the helicon waves extend far from antenna but are very weak. The plasma load resistance grows with density and saturates when the countercurrent is strong enough to cancel the antenna magnetic flux in the bulk plasma. The saturation level is weakly sensitive to whereas the saturation density increases with the magnetic field. Thus, in highly collisional helicon plasma the skin effect arises due to strongly damped electrostatic TG waves rather than due to evanescent electromagnetic fields as is the case in ICP plasmas and in magnetized plasmas excited by axially uniform rf field. A good agreement of measured and computed plasma load resistances corroborates the reasonability of these arguments.

Acknowledgments

We thank Prof. Y. Kawai for his continuous encouragement. This work was partly supported by the Casio Science Promotion Foundation.

References

[1] R.W. Boswell, F.F. Chen, IEEE Trans. Plasma Sci. 25 (1997) 1229.
[2] F.F. Chen, R.W. Boswell, IEEE Trans. Plasma Sci. 25 (1997) 1245.
[3] T. Mieno, T. Shoji, K. Kadota, Appl. Phys. Lett. 59 (1991) 2675.
[4] G. Giroult-Matlakowski, C. Charles, A. Durandet, R. Boswell, S. Armand, H.M. Persing, A.J. Perry, P.D. Loyd, D. Hyde, D. Bogsanyi, J. Vac. Sci. Technol. A 12 (1994) 2754.
[5] Y. Nishimoto, N. Tokumasu, K. Maeda, Jpn. J. Appl. Phys. 34 (1995) 762.
[6] A. Granier, F. Nicolazo, C. Vallée, A. Goullet, G. Turban, B. Grolleau, Plasma Source Sci. Technol. 6 (1997) 147.
[7] D.R. McKenzie, W.D. McFall, H. Smith, B. Higgins, R.W. Boswell, A. Durandet, B.W. James, I.S. Falconer, Nucl. Instrum. Methods B 106 (1995) 90.
[8] S.-H. Kim, I.-H. Kim, K.-S. Kim, J. Vac. Sci. Technol. A 15 (1997) 307.
[9] J.Q. Zhang, Y. Setsuhara, S. Miyake, B. Kyoh, Jpn. J. Appl. Phys. 36 (1997) 6894.
[10] S.-M. Yun, H.-Y. Chang, K.-M. Lee, D.-C. Kim, C.-K. Choi, J. Electrochem. Soc. 145 (1998) 2576.
[11] X. Wang, H. Masumoto, Y. Someno, T. Hirai, J. Vac. Sci. Technol. A 16 (1998) 2926.
[12] M.A. Lieberman, A.J. Lichtenberg, Principles of Plasma Discharges and Materials Processing, John Wiley & Sons, Inc, New York, 1994.
[13] K.P. Shamrai, V.P. Pavlenko, V.B. Taranov, Plasma Phys. Control. Fusion 39 (1997) 505.
[14] D. Arnush, F.F. Chen, Phys. Plasmas 5 (1998) 1239.
[15] S. Shinohara, N. Kaneda, Y. Kawai, Thin Solid Films 316 (1998) 139.
[16] S. Shinohara, K.P. Shamrai, Plasma Phys. Control. Fusion 42 (2000) 865.
[17] S. Shinohara, K. Yonekura, Plasma Phys. Control. Fusion 42 (2000) 41.
[18] T.H. Stix, Theory of Plasma Waves, McGraw-Hill, New York, 1962.
[19] K.P. Shamrai, S. Shinohara, Phys. Plasmas 8 (2001) 4659.